Gate-controlled quantum dots in monolayer WSe_2

Boddison-Chouinard, Justin; Bogan, Alex; Fong, Norman; Watanabe, Kenji; Taniguchi, Takashi; Studenikin, Sergei; Sachrajda, Andrew; Korkusinski, Marek; Altintas, Abdulmenaf; Bieniek, Maciej; Hawrylak, Pawel; Luican-Mayer, Adina; Gaudreau, Louis

Publisher's version / Version de l'éditeur:
https://doi.org/10.1063/5.0062838
Applied Physics Letters, 119, 13, pp. 1-5, 2021-09-28

Applied Physics Letters

Gate-controlled quantum dots in monolayer WSe_2

Cite as: Appl. Phys. Lett. **119**, 133104 (2021); https://doi.org/10.1063/5.0062838
Submitted: 08 July 2021 • Accepted: 13 September 2021 • Published Online: 28 September 2021

Justin Boddison-Chouinard, Alex Bogan, Norman Fong, et al.

Applied Physics Letters ARTICLE scitation.org/journal/apl

Gate-controlled quantum dots in monolayer WSe_2

Cite as: Appl. Phys. Lett. **119**, 133104 (2021); doi: 10.1063/5.0062838
Submitted: 8 July 2021 · Accepted: 13 September 2021 ·
Published Online: 28 September 2021

View Online Export Citation CrossMark

Justin Boddison-Chouinard,[1] Alex Bogan,[2] Norman Fong,[2] Kenji Watanabe,[3] Takashi Taniguchi,[4] Sergei Studenikin,[2] Andrew Sachrajda,[2] Marek Korkusinski,[2] Abdulmenaf Altintas,[1] Maciej Bieniek,[1,5] Pawel Hawrylak,[1] Adina Luican-Mayer,[1,a)] and Louis Gaudreau[2,a)]

AFFILIATIONS

[1]Department of Physics, University of Ottawa, Ottawa, Ontario K1N 9A7, Canada
[2]Emerging Technologies Division, National Research Council of Canada, Ottawa, Ontario K1A 0R6, Canada
[3]Research Center for Functional Materials, National Institute for Materials Science, 1-1 Namiki, Tsukuba 305-0044, Japan
[4]International Center for Materials Nanoarchitectonics, National Institute for Materials Science, 1-1 Namiki, Tsukuba 305-0044, Japan
[5]Department of Theoretical Physics, Wroclaw University of Science and Technology, Wroclaw, Poland

Note: This paper is part of the APL Special Collection on Emerging Qubit Systems - Novel Materials, Encodings and Architectures.
[a)]**Author to whom correspondence should be addressed:** luican-mayer@uottawa.ca and Louis.Gaudreau@nrc-cnrc.gc.ca

ABSTRACT

Quantum confinement and manipulation of charge carriers are critical for achieving devices practical for quantum technologies. The interplay between electron spin and valley, as well as the possibility to address their quantum states electrically and optically, makes two-dimensional (2D) transition metal dichalcogenides an emerging platform for the development of quantum devices. In this work, we fabricate devices based on heterostructures of layered 2D materials, in which we realize gate-controlled tungsten diselenide (WSe_2) hole quantum dots. We discuss the observed mesoscopic transport features related to the emergence of quantum dots in the WSe_2 device channel, and we compare them to a theoretical model.

One of the most promising solid-state platforms for implementing qubits is based on semiconductor spin qubits utilizing the spin degree of freedom of electrostatically confined electrons in semiconductors.[1,2] This topic has been extensively studied in materials such as GaAs and SiGe, in which researchers have been able to create circuits from one to up to nine quantum dots[3–6] and have successfully demonstrated coherent quantum operations using the spin of the confined carriers.[7,8] Despite significant progress, material specific challenges continue to hamper the development of complex quantum devices. For example, GaAs spin qubits suffer from short coherence times mainly due to the hyperfine interaction with nuclei.[9] SiGe devices have significantly higher qubit coherence times when using purified[28] Si,[10] which has zero nuclear spin. However, the indirect bandgap in Si prevents such devices from performing coherent photon to spin conversion, which is necessary for long distance quantum network communications.[11]

With the development of advanced methods for fabricating 2D materials heterostructures, devices based on atomically thin semiconducting transition metal dichalcogenides (TMDs)[12] are emerging as a promising platform in the field of quantum information science.[13,14] Semiconducting TMDs typically exhibit a direct bandgap at the K-point in the Brillouin zone.[15] Moreover, they have potential for realizing spin qubits with long coherence time due to spin-valley locking, caused by the strong spin–orbit interaction and the symmetries of their 2D lattice.[16] These promising properties motivated recent efforts to understand charge transport through quantum dots in 2D materials.[17–21] Gated structures were used to create many-electron single and double quantum dots in eight layers of molybdenum disulfide (MoS_2),[18] in monolayer MoS_2,[19] as well as in monolayer and bilayer tungsten diselenide (WSe_2).[21] In these low-dimensional structures, defects and disorder affect the transport properties of real devices, where they alter the electrostatic environment experienced by the charge carriers.[22,23] Effects of such a potential landscape have been seen in experiments reporting resonant transport through quantum dots that form in local minima.[24,25] These experiments underscore not only the promise of the 2D materials platform for quantum devices but also the remaining challenges in material purity, device fabrication and ultimate electrical and optical control over the charge, and spin and valleys' degrees of freedom of the quantum states. Here, we address some of these questions and present measurements of hole transport through a monolayer WSe_2 quantum dot. Our approach, which differs from similar reported devices,[21] allows us to identify and

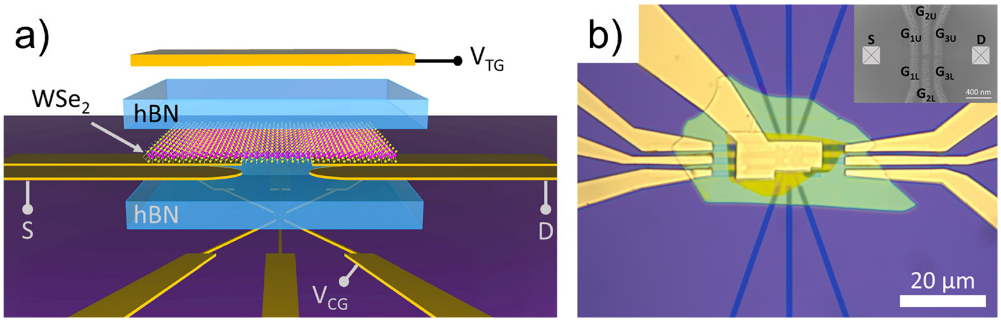

FIG. 1. (a) Schematic of the monolayer WSe_2 device structure. Cr (2 nm)/Pt (8 nm) contacts are used to contact monolayer WSe_2 from the bottom. HBN encapsulates the WSe_2 layer, while a top gate (V_{TG}) and bottom control gates (V_{CG}) are used to control the carrier density in the WSe_2 layer. (b) Optical micrograph of a competed device. The inset represents a scanning electron micrograph depicting the layout of the control gates.

control, using gates, quantum dots formed in the local minima of electrostatic potential fluctuations in monolayer WSe_2 at a temperature of 4 K. We estimate the charging energy and diameter of the dot using a simple capacitive model, and we present a numerical model of quantum dots in this material.

The WSe_2 device was assembled using standard dry transfer methods[26–28] on a Si/SiO_2 wafer with 285 nm SiO_2 and degenerately doped Si. A schematic representation and an optical micrograph of a completed device are shown in Fig. 1. Hexagonal boron nitride (hBN) (38 nm), used as an insulating dielectric, was transferred on top of pre-patterned local control gates [Ti (2.5 nm)/Au (2.5 nm)], followed by patterned bottom electrical contacts [Cr (2 nm)/Pt (8 nm)][29] using e-beam lithography. To minimize the contact resistance, we mechanically removed the polymer residues using an atomic force microscope tip in the contact mode.[30,31] Following this key step, we used dry transfer techniques to position a WSe_2 monolayer encapsulated by a hBN flake ($\approx$30 nm) onto the mechanically cleaned bottom contacts. In a final lithographic step, we deposited a top gate [Ti (5 nm)/Pd (20 nm)/Au (100 nm)], which covered the entire WSe_2 flake. This gate was used to modify the charge carrier density in WSe_2 and to achieve a regime of the ohmic contact. Details of device fabrication and cleaning are presented in the supplementary material.

Experimental characterization of this device was initially performed by applying a small DC voltage to the source contact and monitoring the drain current, while sweeping a DC voltage on the top gate [Fig. 2(a)]. The increase in current for negative top gate voltages indicates the successful population of holes in the channel, consistent with the doping levels found in previous experiments.[21,29] Furthermore, as the temperature is lowered from room temperature to 4 K, a larger negative voltage on the top gate is necessary to activate the conducting channel, as the microscopic crystal defects decrease the device mobility especially at low temperatures.[32] The remaining measurements shown in this Letter are performed at 4 K. Figure 2(b) shows current-voltage characteristics obtained at different values of

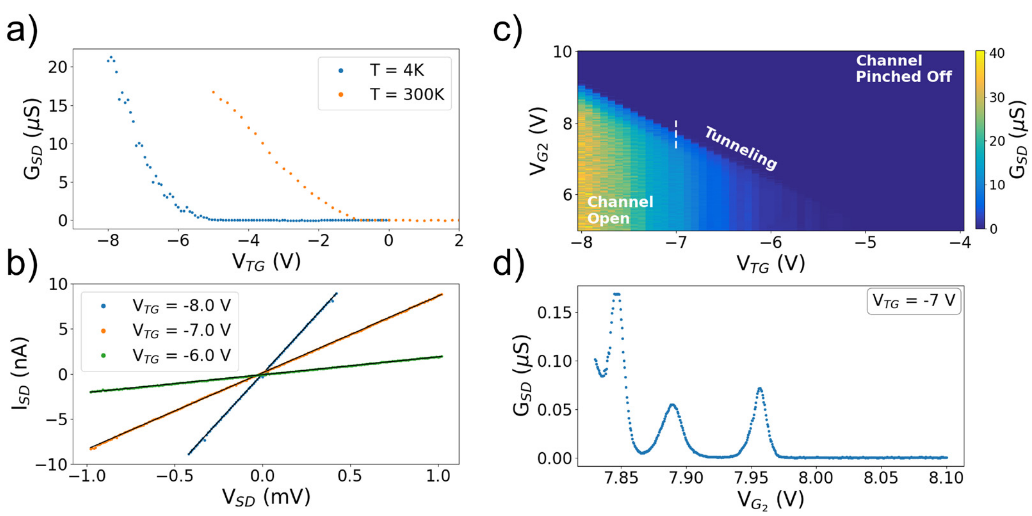

FIG. 2. (a) Source–drain conductance as a function of the top gate voltage, where the orange (blue) curve was taken at room temperature (4 K). (b) Source–drain current vs source–drain voltage taken at various top gate voltages, while all control gates are grounded. (c) Source–drain conductance vs top gate and control gates V_{G2} [upper-middle and lower-middle in the inset of Fig. 1(b)]. The conductance across the channel operates in three distinct regimes: an open channel, a tunneling regime, and a pinched-off regime. (d) Source–drain conductance vs the control gate voltage V_{G2} at a constant top gate voltage of –7 V.

the top gate voltage, as indicated. We note that in our device ohmic contacts are achieved when the top gate is tuned below –5 V, as evidenced by the linear behavior of the $I_{SD}-V_{SD}$ curves. A total resistance of 47 kΩ is observed at a top gate voltage of $V_{TG} = -8$ V.

Next, we investigated the influence of the local control gates on the transport proprieties of the device, by applying identical voltages to a pair of control gates [upper (U) and lower (L)], while keeping the remaining control gates grounded. Figure 2(c) shows the conductivity G_{SD} across the WSe_2 channel as a function of the top gate voltage V_{TG} and the voltage applied to both control gates in the pair G_{2U} and G_{2L} simultaneously, V_{G2}. We distinguish three regimes. When the channel is activated by the top gate and the control gate voltages are below a certain threshold, the channel is open (conductive), and a finite current is measured. As we increase the local control gate voltage V_{G2}, the channel crosses over to a resonant tunneling regime and is eventually completely pinched-off with sufficiently large control gate voltages. For clarity, Fig. 2(d) shows a line trace along the range of voltages indicated by the dashed line in Fig. 2(c), taken at a top gate voltage $V_{TG} = -7$ V. The presence of resonant transport peaks in the tunneling regime suggests the presence of quantum dots in the device.

We can further explore the characteristics of the quantum dots in the channel by varying the voltages on the local control gates. Figure 3(a) shows the changes in the source–drain current I_{SD}, when we vary the voltages on G_{2U} and G_{2L}, at a fixed top gate voltage $V_{TG} = -5.5$ V. In this charge stability diagram, we identify horizontal lines and vertical lines, corresponding to different transport resonances through quantum dots. Vertical lines indicate that the quantum dot is capacitively coupled only to gate G_{2U} and, therefore, that its location is under the gate G_{2U} or very close to it. Similarly, horizontal peaks are entirely controlled by gate G_{2L}. We can also identify quantum dots formed in between gates as depicted by the G_{3L}-G_{3U} stability diagram in Fig. 3(b), where in addition to having horizontal and vertical lines, we find diagonal lines with various slopes, indicating the presence of quantum dots forming at various locations between the two gates. In this situation, we observe avoided crossings as the one highlighted in the inset of Fig. 3(b), suggesting capacitive coupling between such quantum dots. The results presented in both Figs. 3(a) and 3(b) imply that the potential landscape of the WSe_2 varies across the sample, creating local quantum dots that are identified by transport resonances near depletion. The control gates can, therefore, be used to study individual quantum dots.

We explore the properties of the quantum dot associated with the vertical lines in Fig. 3(a), by sweeping the bias voltage V_{SD} for different values of G_{2L} and G_{2U} as indicated by the dashed line, while the top gate voltage is kept constant $V_{TG} = -5.5$ V. The variation of the source-drain current I_{SD} while the bias and control gate voltages are varied is shown in Fig. 3(c). We note the presence of diamond-shaped feature (Coulomb diamonds) characteristics of quantum dot behavior, where regions with zero source–drain current represent a regime of Coulomb blockaded transport. From the plot of Fig. 3(c), we can estimate the size and charging energy of the quantum dot. From the height of the first Coulomb diamond, the charging energy $U \sim 3.4$ meV, value consistent with previous reports in gated QD structures in WSe_2.[21,24] Figure 3(d) shows a line cut through the map of Fig. 3(c), taken at a source-drain voltage $V_{SD} = 154$ μV. The energy separation between the peaks is $\Delta V_G \approx 65$ mV. We can estimate the size of the quantum

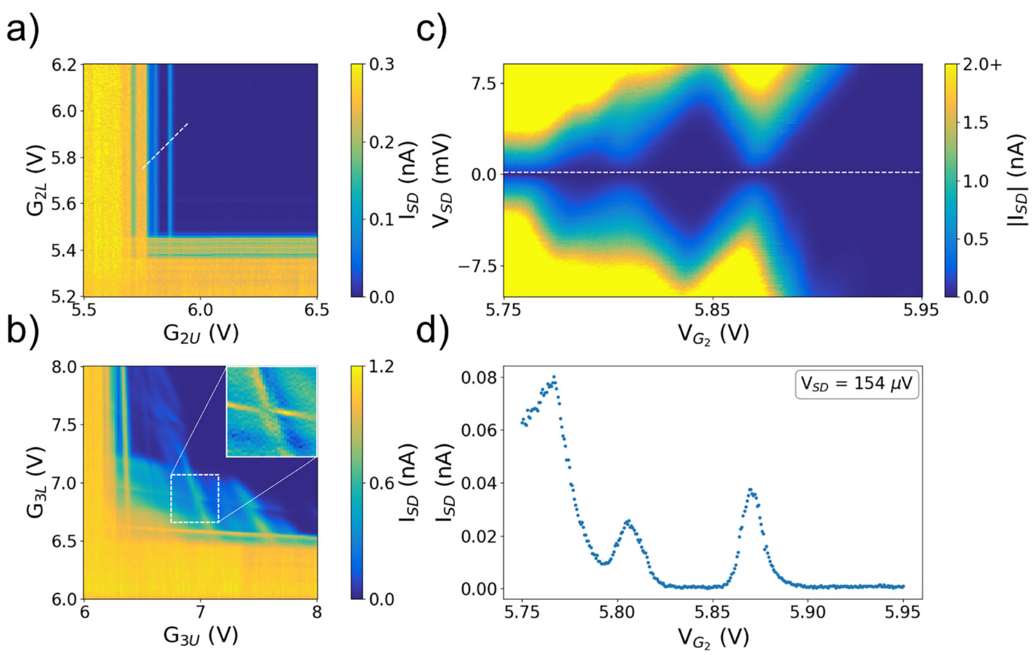

FIG. 3. (a) Source–drain current I_{SD} as a function of individual control gates G_{2L} and G_{2U} taken at $V_{TG} = -5.5$ V and $V_{SD} = 0.5$ mV. (b) Source–drain current I_{SD} as a function of two other individual control gates G_{3L} and G_{3U} taken at $V_{TG} = -6.0$ V and $V_{SD} = 0.5$ mV. The inset represents the derivative $\partial I_{SD}/\partial G_{3L}$ of the white dashed box. (c) Source–drain current I_{SD} as a function of bias voltage V_{SD} and control gate V_{G2} voltage corresponding to the white dashed line in (a). (d) Source-drain current I_{SD} as a function of $G_{2L\&R}$ taken at a $V_{SD} = 154$ μV corresponding to the white dashed line in (c).

dot by approximating the quantum dot and the control gate as a parallel plate capacitor, as detailed in the supplementary material. Using $\epsilon_{hBN} = 4$ as hBN's relative permittivity[33] and its thickness $t_{hBN} = 38$ nm, the gate capacitance is approximated to be $C_G = \epsilon_0\epsilon_{hBN}\pi d^2/4t_{hBN}$, where d is the quantum dot diameter. The gate capacitance can also be expressed as $C_G = e^2/\Delta V_G$. From these two equations, we estimate the quantum dot diameter to be $d \approx 58$ nm.

To understand the nature of electronic states available for holes that are confined in a WSe_2 quantum dot as well as the interplay of valley, spin, and orbital degrees of freedom, we performed tight binding and *ab initio* calculations (using ABINIT) of valence holes in single layer WSe_2[34,35] and confined to a gated quantum dot.[35–37] A single layer of WSe_2 consists of two triangular sublattices: sublattice A, having d-orbitals from W atoms and sublattice B, consisting of a pair of Se atoms with *p*-orbitals below and above the metal layer. A WSe_2 monolayer with such a hexagonal lattice is a direct gap semiconductor with energy minima at the two nonequivalent valleys in the Brillouin zone. Figure 4(a) shows the calculated energy spectrum of holes in a single layer of WSe_2 around the two nonequivalent valleys, $+K$ and $-K$, where the strong spin–orbit interaction leads to splitting of hole spin up and spin down states by 470 meV. This implies that the spin degree of freedom of the hole ground states is locked to the valley index with spin up locked to $+K$ and spin down locked to $-K$. In addition, the hole wavefunction changes its orbital character, at $+K$ valley it is built of $m = +2$ W d-orbital, where d-orbital corresponds to the state with angular momentum $l = 2$ and z-projections $m = 0, \pm 2$,[34] while at $-K$ valley, it is built of $m = -2$ W d-orbital. The energy bands reflect the massive Dirac fermion description of the energy bands in WSe_2, where close to the top of the upper valence band, the dispersion is approximately parabolic with effective mass $m^* = 0.28$, but it quickly becomes linear.

We consider hole states localized in a WSe_2 quantum dot, similar to those leading to the observed Coulomb blockade spectrum in our device. Figure 4(b) represents an idealized Gaussian potential profile generated by an external gate[35,37] with $V_0 = 100$ meV and a diameter of 60 nm, assumed to confine hole states in a WSe_2 layer. The calculated spectrum for this quantum dot is shown in Fig. 4(c), where the zero energy is at the top of the valence band and the confining potential leads to discrete quantum dot levels in the energy gap of the WSe_2 layer. As a result of confinement, we find several energy shells, separated by energy $\omega_0 = 5$ meV. The lowest hole energy s-shell is doubly degenerate, corresponding to $(+K, \uparrow, m = +2)$ and $(-K, \downarrow, m = -2)$ states. The next energy p-shell is almost fourfold degenerate, followed by a sixfold degenerate d-shell. The predicted hole energy spectrum is similar to the energy spectrum of carriers confined to semiconductor parabolic quantum dots,[38] except for lifting the degeneracy of hole shells by topological magnetic moments inherent to massive Dirac fermions.[35–37] To estimate the charging energy U needed to add a hole to the lowest state, we consider a parabolic quantum dot, so that $U = Ry^*\sqrt{\pi}\sqrt{\omega_0/Ry^*}$,[39] where Ry^* is an effective Rydberg, given by $Ry^* = Ry \times m^*/(\epsilon^2)$, where m^* is the effective mass and ϵ is the effective dielectric constant. For typical parameters $\epsilon = 10$ and $m^* = 0.28$ characteristic of holes in WSe_2, the resulting charging energy is found to be $U = 20$ meV. We note that the discrepancy between this simple model and the measured experimental results is likely due to the presence of random electrostatic potential below the semiconducting channel or the gate, as schematically illustrated in Fig. 4(d). This suggests that to fully take advantage of the unique properties of quantum confined states in 2D semiconductors, more effort is needed to optimize the materials homogeneity and purity, as well as to improve electrical contacts.

In summary, we demonstrated electrical control of WSe_2 hole quantum dots in gated devices based on 2D heterostructures. Electrical transport measurements revealed a Coulomb blockade regime, from which we estimated the charging energy and size of the formed quantum dots. Additionally, charge stability diagrams using

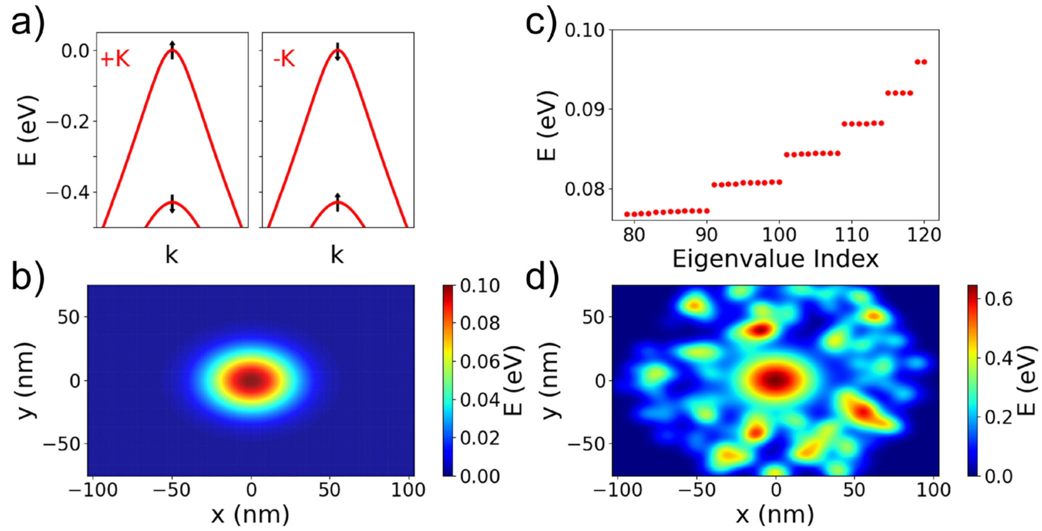

FIG. 4. (a) Electronic band dispersion for WSe_2 around the top of the valence band for the two valleys $+K$ and $-K$, emphasizing the spin structure. (b) Schematic view of a simulated Gaussian potential for a quantum dot in WSe_2. (c) Energy spectrum of hole states in a WSe_2 quantum dot confined by the potential shown in (b). (d) Schematic representation of a quantum dot generated by a gate and surrounded by a random electrostatic potential.

control gates indicate that the quantum dots are likely generated by the inherent electrostatic fluctuations of the device, and they can be coupled. Our theoretical calculations reveal that the ground state of holes in such a quantum dot is not fourfold degenerate as expected and found in bilayer graphene quantum dots,[17] due to the spin and valley degrees of freedom, but doubly degenerate due to valley-spin locking. These results shed light on mesoscopic transport features in 2D semiconducting quantum dot devices, paving the way for the development of quantum devices based on electrostatically confined WSe_2 quantum dots.

See the supplementary material for details on device fabrication and AFM cleaning as well as for quantum dot size calculations.

The authors thank A. Dusko and Y. Saleem for useful discussions. This work was supported by the High Throughput and Secure Networks Challenge Program at the National Research Council of Canada. A.L.-M. and J.B.-C. acknowledge funding from the National Sciences and Engineering Research Council (NSERC) Discovery Grant No. RGPIN-2016-06717. We also acknowledge the support of the Natural Sciences and Engineering Research Council of Canada (NSERC) through Strategic Project No. STPGP 521420. P.H. and A.A. acknowledge NSERC Discovery grant and University of Ottawa Research Chair in Quantum Theory of Materials, Nanostructures, and Devices. M.B. acknowledges financial support from the Polish National Agency for Academic Exchange (NAWA), Poland, Grant No. PPI/APM/2019/1/00085/U/00001. Computing resources from Compute Canada are gratefully acknowledged. K.W. and T.T. acknowledge support from the Elemental Strategy Initiative conducted by the MEXT, Japan (Grant No. JPMXP0112101001) and JSPS KAKENHI (Grant Nos. 19H05790 and JP20H00354).

DATA AVAILABILITY

The data that support the findings of this study are available from the corresponding authors upon reasonable request.

REFERENCES

1. J. A. Brum and P. Hawrylak, Superlattices Microstruct. **22**, 431 (1997).
2. D. Loss and D. P. DiVincenzo, Phys. Rev. A **57**, 120 (1998).
3. M. Ciorga, A. S. Sachrajda, P. Hawrylak, C. Gould, P. Zawadzki, S. Jullian, Y. Feng, and Z. Wasilewski, Phys. Rev. B **61**, R16315 (2000).
4. J. M. Elzerman, R. Hanson, J. S. Greidanus, L. H. W. van Beveren, S. D. Franceschi, L. M. K. Vandersypen, S. Tarucha, and L. P. Kouwenhoven, Phys. Rev. B **67**, 161308 (2003).
5. L. Gaudreau, A. Kam, G. Granger, S. A. Studenikin, P. Zawadzki, and A. S. Sachrajda, Appl. Phys. Lett. **95**, 193101 (2009).
6. D. Zajac, T. Hazard, X. Mi, E. Nielsen, and J. Petta, Phys. Rev. Appl. **6**, 054013 (2016).
7. J. M. Nichol, L. A. Orona, S. P. Harvey, S. Fallahi, G. C. Gardner, M. J. Manfra, and A. Yacoby, npj Quantum Inf. **3**, 3 (2017).
8. D. M. Zajac, A. J. Sigillito, M. Russ, F. Borjans, J. M. Taylor, G. Burkard, and J. R. Petta, Science **359**, 439 (2018).
9. R. Hanson, L. P. Kouwenhoven, J. R. Petta, S. Tarucha, and L. M. K. Vandersypen, Rev. Mod. Phys. **79**, 1217 (2007).
10. M. Veldhorst, J. C. C. Hwang, C. H. Yang, A. W. Leenstra, B. de Ronde, J. P. Dehollain, J. T. Muhonen, F. E. Hudson, K. M. Itoh, A. Morello, and A. S. Dzurak, Nat. Nanotechnol. **9**, 981 (2014).
11. P. Lodahl, Quantum Sci. Technol. **3**, 013001 (2018).
12. A. K. Geim and I. V. Grigorieva, Nature **499**, 419 (2013).
13. M. Atatüre, D. Englund, N. Vamivakas, S.-Y. Lee, and J. Wrachtrup, Nat. Rev. Mater. **3**, 38 (2018).
14. X. Liu and M. C. Hersam, Nat. Rev. Mater. **4**, 669 (2019).
15. K. F. Mak, C. Lee, J. Hone, J. Shan, and T. F. Heinz, Phys. Rev. Lett. **105**, 136805 (2010).
16. A. Kormányos, V. Zólyomi, N. D. Drummond, and G. Burkard, Phys. Rev. X **4**, 039901 (2014).
17. R. Pisoni, Y. Lee, H. Overweg, M. Eich, P. Simonet, K. Watanabe, T. Taniguchi, R. Gorbachev, T. Ihn, and K. Ensslin, Nano Lett. **17**, 5008 (2017).
18. Z.-Z. Zhang, X.-X. Song, G. Luo, G.-W. Deng, V. Mosallanejad, T. Taniguchi, K. Watanabe, H.-O. Li, G. Cao, G.-C. Guo, F. Nori, and G.-P. Guo, Sci. Adv. **3**, e1701699 (2017).
19. R. Pisoni, Z. Lei, P. Back, M. Eich, H. Overweg, Y. Lee, K. Watanabe, T. Taniguchi, T. Ihn, and K. Ensslin, Appl. Phys. Lett. **112**, 123101 (2018).
20. K. Wang, K. D. Greve, L. A. Jauregui, A. Sushko, A. High, Y. Zhou, G. Scuri, T. Taniguchi, K. Watanabe, M. D. Lukin, H. Park, and P. Kim, Nat. Nanotechnol. **13**, 128 (2018).
21. S. Davari, J. Stacy, A. Mercado, J. Tull, R. Basnet, K. Pandey, K. Watanabe, T. Taniguchi, J. Hu, and H. Churchill, Phys. Rev. Appl. **13**, 054058 (2020).
22. D. Rhodes, S. H. Chae, R. Ribeiro-Palau, and J. Hone, Nat. Mater. **18**, 541 (2019).
23. R. Plumadore, M. Baskurt, J. Boddison-Chouinard, G. Lopinski, M. Modarresi, P. Potasz, P. Hawrylak, H. Sahin, F. M. Peeters, and A. Luican-Mayer, Phys. Rev. B **102**, 205408 (2020).
24. X.-X. Song, D. Liu, V. Mosallanejad, J. You, T.-Y. Han, D.-T. Chen, H.-O. Li, G. Cao, M. Xiao, G.-C. Guo, and G.-P. Guo, Nanoscale **7**, 16867 (2015).
25. X.-X. Song, Z.-Z. Zhang, J. You, D. Liu, H.-O. Li, G. Cao, M. Xiao, and G.-P. Guo, Sci. Rep. **5**, 16113 (2015).
26. L. Wang, I. Meric, P. Y. Huang, Q. Gao, Y. Gao, H. Tran, T. Taniguchi, K. Watanabe, L. M. Campos, D. A. Muller, J. Guo, P. Kim, J. Hone, K. L. Shepard, and C. R. Dean, Science **342**, 614 (2013).
27. J. Boddison-Chouinard, R. Plumadore, and A. Luican-Mayer, J. Visualized Exp. **149**, e59727 (2019).
28. J. Boddison-Chouinard, S. Scarfe, K. Watanabe, T. Taniguchi, and A. Luican-Mayer, Appl. Phys. Lett. **115**, 231603 (2019).
29. H. C. P. Movva, A. Rai, S. Kang, K. Kim, B. Fallahazad, T. Taniguchi, K. Watanabe, E. Tutuc, and S. K. Banerjee, ACS Nano **9**, 10402 (2015).
30. A. M. Goossens, V. E. Calado, A. Barreiro, K. Watanabe, T. Taniguchi, and L. M. K. Vandersypen, Appl. Phys. Lett. **100**, 073110 (2012).
31. M. R. Rosenberger, H.-J. Chuang, K. M. McCreary, A. T. Hanbicki, S. V. Sivaram, and B. T. Jonker, ACS Appl. Mater. Interfaces **10**, 10379 (2018).
32. N. Pradhan, D. Rhodes, S. Memaran, J. Poumirol, D. Smirnov, S. Talapatra, S. Feng, N. Perea-Lopez, A. Elias, M. Terrones *et al.*, Sci. Rep. **5**, 08979 (2015).
33. A. F. Young, C. R. Dean, I. Meric, S. Sorgenfrei, H. Ren, K. Watanabe, T. Taniguchi, J. Hone, K. L. Shepard, and P. Kim, Phys. Rev. B **85**, 235458 (2012).
34. M. Bieniek, M. Korkusiński, L. Szulakowska, P. Potasz, I. Ozfidan, and P. Hawrylak, Phys. Rev. B **97**, 085153 (2018).
35. A. Alt intaş, M. Bieniek, A. Dusko, M. Korkusiński, J. Pawłowski, and P. Hawrylak, arXiv:2106.15090 (2021).
36. M. Bieniek, L. Szulakowska, and P. Hawrylak, Phys. Rev. B **101**, 035401 (2020).
37. L. Szulakowska, M. Cygorek, M. Bieniek, and P. Hawrylak, Phys. Rev. B **102**, 245410 (2020).
38. S. Raymond, S. Studenikin, A. Sachrajda, Z. Wasilewski, S.-J. Cheng, W. Sheng, P. Hawrylak, A. Babinski, M. Potemski, G. Ortner *et al.*, Phys. Rev. Lett. **92**, 187402 (2004).
39. M. Korkusinski, W. Sheng, and P. Hawrylak, Phys. Status Solidi (b) **238**, 246 (2003).